Deposition of small particles from turbulent flows

Z. Wu & J. B. Young
Hopkinson Laboratory, Cambridge University Engineering Department

Abstract

This paper deals with particle deposition onto solid walls from turbulent flows. The aim of the study is to model particle deposition in industrial flows, such as the one in gas turbines. The numerical study has been carried out with a two fluid approach. The possible contribution to the deposition from Brownian diffusion, turbulent diffusion and shear-induced lift force are considered in the study. Three types of turbulent two-phase flows have been studied: turbulent channel flow, turbulent flow in a bent duct and turbulent flow in a turbine blade cascade. The results show that the current two fluid models are capable of predicting particle deposition rates in complex industrial flows.

1 Introduction

Numerical study of particle dispersion/deposition in turbulent flows has traditionally been carried out using two approaches: Lagrangian approach and Eulerian approach. In the Lagrangian approach, particles are tracked individually within the flow domain by integrating the particle equation of motion, and a large number of particles have to be modelled to obtain good statistics. The alternative is the Eulerian approach. In this method, particles are treated as continuous fluid, and the motion of the particles is mathematically described by mass, momentum and energy conservation, similar to a fluid. In the Eulerian approach, tracking of individual particles is avoided, which make this approach much more efficient than the Lagrangian one. But the method has its own difficulties. For inertial particle transport and deposition problems, discontinuities may exist in the particulate flow field, which are difficult to predict. What is more, it is quite difficult to define the wall boundary conditions for a wall-confined flow. Despite all the disadvantages, the Eulerian approach is

Advances in Fluid Mechanics V, A. Mendes, M. Rahman & C. A. Brebbia (Editors)

selected in the current study, since computational efficiency is the prerequisite for industrial use.

The deposition of small particles in turbulent flows onto solid walls has been well researched, but mainly on simple geometries such as pipes and channels. These researches provide us with considerable knowledge on this topic. One major parameter in studying particle deposition is the particle response time which characterizes the dynamics of particle motion:

$$\tau_p = \frac{\rho_{mat} d_p^2}{18 \rho_g \nu_g}(1 + 2.7Kn) \tag{1}$$

where, ρ_{mat} is the particle material density, d_p is the particle diameter, ρ_g is the gas density, ν_g is the gas kinematic viscosity, $Kn=\lambda_g/d_p$ is the particle Knudsen number, λ_g being the mean free path of a gas molecule. The factor $(1+2.7Kn)$ is used to correct for deviations from continuum behaviour when the particle diameter is comparable with the mean free path of a gas molecule. τ_p is often non-dimensionlised by the wall friction velocity u^* and the particle kinematic viscosity ν_g:

$$\tau_p^+ = \frac{\tau_p u^{*2}}{\nu_g} \tag{2}$$

The particle deposition processes in turbulent pipe flows are usually divided into three regimes (Young & Leeming [7]): the diffusional deposition regime, the diffusion-impaction regime and the inertia-moderate regime. In the diffusional regime, small particles ($\tau_p^+<0.2$) are transported to the wall by turbulent diffusion, and at a distance that is very close to the wall (viscous sub layer), particles are driven by the Brownian force until they reach the wall. For particles with reasonably large inertia ($0.2<\tau_p^+<2$), the final step of the deposition relies on the particle inertia gained from the fluid turbulence, and the diffusion-impaction regime applies. Particles with large inertia ($\tau_p^+>2$) will be less responsive to the fluid turbulence, and this results in a decreasing trend of deposition rate, known as the inertia-moderate regime. These regimes can be seen clearly from previous experimental data on particle deposition in turbulent pipe flows. See Fig. 1. The dimensionless particle deposition rate is defined as the mass flux at the wall, divided by a mean particle density. It is then made dimensionless using the friction velocity:

$$V_d^+ = \frac{J_W}{\overline{\rho}_{p,mean} u^*} \tag{3}$$

In turbulent pipe flows, particle deposition takes place upon surfaces parallel to the flow, by turbulent transportation. When a turbine cascade is considered, the deposition problem becomes complicated. On the one hand, the flow field and turbulence of the gas phase become complex, this will in turn create complexity in the statistics of the particle motion. On the other hand, the existence of

Advances in Fluid Mechanics V, A. Mendes, M. Rahman & C. A. Brebbia (Editors)

curvature in a complex geometry, bring the particle inertia to a more important position. At certain particle sizes, the effect of particle inertia due to the effect of the streamlines may compete with the turbulent transportation, and makes the deposition process much more complicated than in turbulent pipe/channel flows. In this paper, flows involving the curvature effect are studied. Deposition rates in a curved duct and a cascade of turbine blades are predicted.

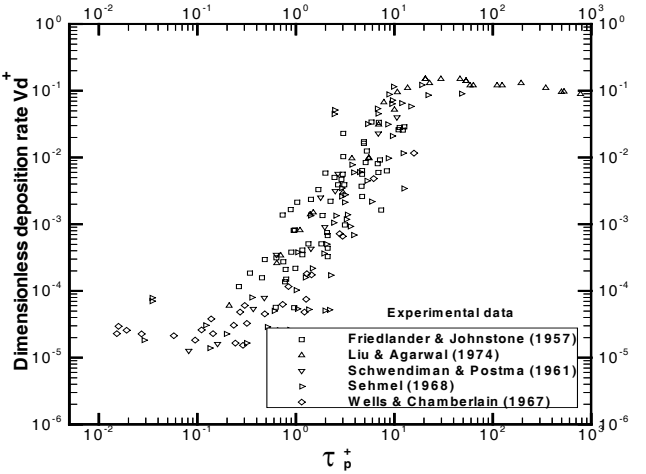

Figure 1: Particle deposition in fully developed turbulent pipe flows.

2 Theory

In the current study, a set of ensemble-averaged equations is used to describe the transport of the mass and momentum of the particles. The derivation of the equations and the modelling of the particle turbulence correlation is a complex process which is not described here. Full details can be found in Slater et al. [5]. The gas-phase velocity u_i is decomposed into an ensemble-averaged and a fluctuating component,

$$u_i = \overline{U_i} + u_i' \tag{4}$$

Similar decomposition is used for the particle density ρ_p,

$$\rho_p = \overline{\rho_p} + \rho_p' \tag{5}$$

The particle velocity v_i is decomposed into a density-weighted average and a fluctuating component,

$$v_i = \overline{\overline{V_i}} + v_i'' \tag{6}$$

The particle mass conservation equation then takes the form:

$$\frac{\partial \overline{\rho}_p}{\partial t} + \frac{\partial \overline{\rho}_p \overline{\overline{V}_i}}{\partial x_i} - \frac{\partial}{\partial x_i}\left[\left(D_B + D_T\right) \frac{\partial \overline{\rho}_p}{\partial x_i} \right] = 0 \tag{7}$$

Advances in Fluid Mechanics V, A. Mendes, M. Rahman & C. A. Brebbia (Editors)

D_B and D_T are particle Brownian and turbulent diffusion coefficients, respectively.

The particle momentum equation takes the form:

$$\frac{\partial \overline{\rho}_p \overline{\overline{V}}_i}{\partial t} + \frac{\partial \overline{\rho}_p \overline{\overline{V}}_i \overline{\overline{V}}_j}{\partial x_i} = \frac{\overline{\rho}_p \left(\overline{U}_i - \overline{\overline{V}}_i\right)}{\tau_p} + \overline{\rho}_p \overline{\overline{F}}_{L,i} - \overline{\rho}_p \frac{\partial}{\partial x_i}\left(\overline{\overline{v_i'' v_j''}}\right) \tag{8}$$

The terms on the right hand side of the momentum equations are the drag force, the lift force and the turbophoretic force. τ_p is the particle response time.

The lift force takes the form:

$$\overline{\overline{F}}_{L,i} = 0.725 \sum_{\substack{k=1 \\ k \neq i}}^{3} \left[\left(\frac{\rho_g}{\rho_{mat}} \tau_p \frac{\partial \overline{U}_k}{\partial x_i} \right)^{1/2} \frac{\left(\overline{U}_k - \overline{\overline{V}}_k\right)}{\tau_p} \right] \tag{9}$$

The particle fluctuating velocity correlations are modeled as follows:

$$\overline{\overline{v_i'' v_j''}} = \frac{\tau_g}{\tau_g + \tau_p} \overline{u_i' u_j'} \tag{10}$$

This is called the local equilibrium model which assumes that particles respond locally to the fluid turbulent motion through the drag. It does not take the particle crossing trajectory effect into account. A more realistic model proposed by Simonin and Viollet [4] includes the effect of crossing trajectories. The previous equation still holds but τ_g is replaced by τ'_g, where

$$\tau'_g = \tau_g \left(1 + C_\beta \frac{|V_r|^2}{\frac{2}{3} k_g} \right) \tag{11}$$

Here V_r is the mean relative velocity between the fluid and the particle, k_g is the fluid turbulent kinetic energy, C_β is a coefficient fixed by experimental data. Simonin & Viollet [4] recommend the value C_β=0.45.

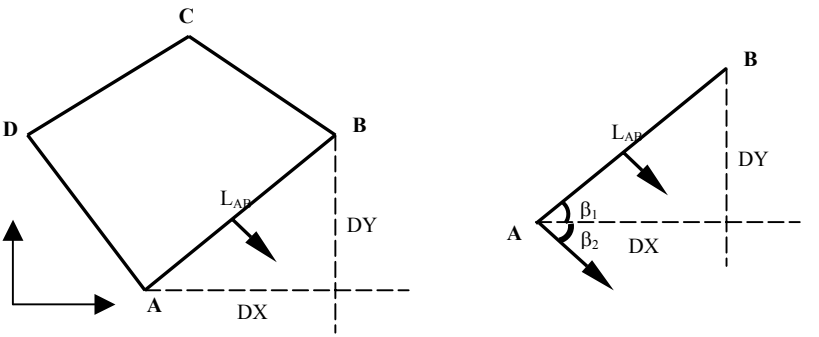

Figure 2.

Advances in Fluid Mechanics V, A. Mendes, M. Rahman & C. A. Brebbia (Editors)

3 The numerical scheme

The above equations are the governing differential equations that apply to the whole particle flow field. The equations now need to be numerically discretized, so they can be numerically solved on each cell in the grid system.

Integrating the above equations and applying Green's theorem, a set of integrated equations are obtained. Applying the integration to each cell across the whole computation domain, the problem is turned into the seeking of the solution of the set of equations that apply to each cell. After discretization, the governing equations of mass and momentum on a typical grid cell (see Fig. 2) are converted to:

$$\frac{\Delta(\overline{\rho}_p)}{\Delta t}\Delta A = -\sum_{i=1}^{4}\left[\overline{\rho}_p * (\overline{\overline{V}}_x * L * NX + \overline{\overline{V}}_y * L * NY)\right]_i + \sum_{i=1}^{4}\left[((D_B + D_T) * \frac{\partial \overline{\rho}_p}{\partial x} L * NX + (D_B + D_T) * \frac{\partial \overline{\rho}_p}{\partial y} L * NY)\right]_i \tag{12}$$

$$\frac{\Delta(\overline{\rho}_p \overline{\overline{V}}_x)}{\Delta t}\Delta A = -\sum_{i=1}^{4}\left[(\overline{\rho}_p \overline{\overline{V}}_x * (\overline{\overline{V}}_x * L * NX + \overline{\overline{V}}_y * L * NY))\right]_i - \sum_{i=1}^{4}\left[\overline{\rho}_p \overline{\overline{v_x'' v_x''}} * L * NX - D_T(\frac{\partial \overline{\overline{V}}_x}{\partial y} + \frac{\partial \overline{\overline{V}}_y}{\partial x}) * L * NY\right]_i + \left[\overline{\rho}_p \frac{(\overline{U}_x - \overline{\overline{V}}_x)}{\tau_p} + \overline{\rho}_p \overline{\overline{F}}_{L,x}\right]\Delta A \tag{13}$$

$$\frac{\Delta(\overline{\rho}_p \overline{\overline{V}}_y)}{\Delta t}\Delta A = -\sum_{i=1}^{4}\left[(\overline{\rho}_p \overline{\overline{V}}_y * (\overline{\overline{V}}_x * L * NX + \overline{\overline{V}}_y * L * NY))\right]_i - \sum_{i=1}^{4}\left[\overline{\rho}_p \overline{\overline{v_y'' v_y''}} * L * NY - D_T(\frac{\partial \overline{\overline{V}}_x}{\partial y} + \frac{\partial \overline{\overline{V}}_y}{\partial x}) * L * NX\right]_i + \left[\overline{\rho}_p \frac{(\overline{U}_y - \overline{\overline{V}}_y)}{\tau_p} + \overline{\rho}_p \overline{\overline{F}}_{L,y}\right]\Delta A \tag{14}$$

Following the above steps and applying the equations to each cell, gives a set of discretized equations. The left hand sides of the equations represent the time derivatives of the unknown variables.

To apply the above discretized equations, a four-stage scheme is used for the time integration, which results in 2nd order accuracy in time. An up-winding scheme is used for the evaluation of the fluxes at the edges, with a space accuracy of 2nd order.

Advances in Fluid Mechanics V, A. Mendes, M. Rahman & C. A. Brebbia (Editors)

4 The boundary conditions

Correct implementation of the boundary conditions is essential for the prediction of flows of the particle phase. It is relatively simple to implement the boundary conditions apart from the one on solid walls. At inlet, the particle velocity components are prescribed. They usually take the values of the gas phase. The particle density is usually set to unity. At outlet, an up-winding extrapolation is used, so that inflow from the outlet is suppressed. At the wall, the boundary condition is physically complex if absorbing and bouncing happen at the same time. Currently, a perfectly absorbing wall is assumed. To implement the wall boundary condition numerically, a first order extrapolation is used for the particle density and velocity components. When the particle velocity is directed towards the wall, this results in a stable scheme. When the particle velocity is directed towards the computational domain, the scheme corresponds to a down-winded flux evaluation, and is unstable. In such cases, zero wall-normal fluxes are set, Slater & Young [6].

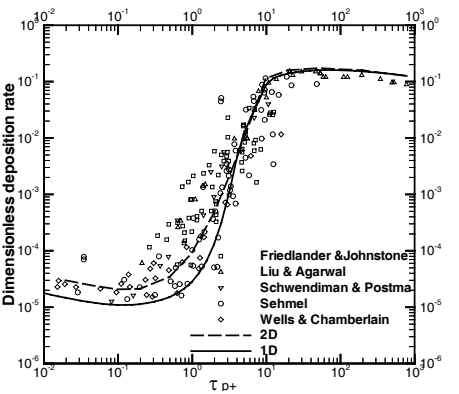

Figure 3.

5 The results

5.1 Deposition in turbulent channel flows

Figure 3 shows the well-known particle deposition curve. The dotted data are those from a variety of experimental works. The current result from the 2-D code is compared with the result of 1-D calculations. The two calculated curves agree with each other well in the inertial deposition range, but the 2-D calculation predicts a higher deposition rate for small particles. Nevertheless, both curves fall within the range of the experimental data.

Advances in Fluid Mechanics V, A. Mendes, M. Rahman & C. A. Brebbia (Editors)

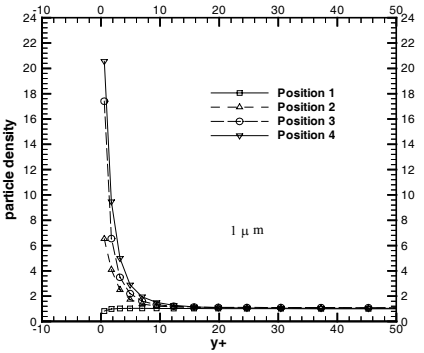

Figure 4: Particle density profile (1 μm).

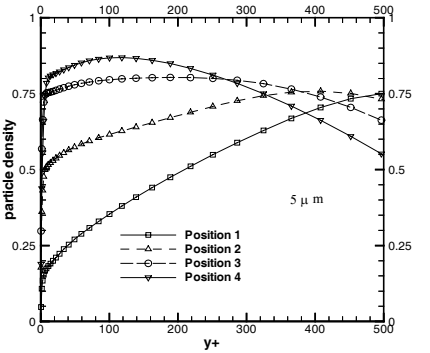

Figure 5: Particle density profile (5 μm).

5.2 Deposition from turbulent flows in a curved duct

The geometry used in this study is a 2D duct of 0.01m width, with a 0.45m straight run before a 45-degree bend and 0.15m after the bend. The gas flow Reynolds Number is Re=20000. The straight pipe length was chosen to allow the particle flow-field to become fully developed upstream of the bend. Thus, an extra 25-channel-width length was added to the straight duct after the gas-phase becomes fully developed (which itself needs around 20 channel widths).

The grid is a single block, with 737 cells in the stream-wise direction and 24 cells across the channel. A non-uniform grid is used which results in a very fine grid close to the wall.

A low Reynolds number k-epsilon model was used to predict the turbulence quantities close to the wall. The turbulent kinetic energy is split into its three components: the mainstream direction, the wall normal direction and the span-wise direction. The split was done according to experimental data for the boundary layer along a smooth wall, as given in the book by Hinze [2]. The friction velocity along the straight part of the channel, after the flow is fully developed, is around u*=1.65 m/s, which is hereafter referred to as the fully developed friction velocity. This u* value, together with the laminar viscosity ν=1.5e-5 m**2/s, is used to make all the other quantities dimensionless. Calculations show that the deposition rate is much influenced by the method of splitting the turbulent kinetic energy into its three components. Currently, with the split scheme described above, reasonable results are obtained.

The particle density is 1150 kg/m**3. 1 μm and 5 μm spherical particles are used in the study. Based on the fully developed friction velocity and the laminar viscosity, the dimensionless particle response time for the two sizes of particle are 0.64 and 16, respectively.

Four cross sections are selected from the simulation. Position 1 is at the beginning of the bend, position 2 is at 30 degree of the bend, position 3 is at the end of the bend, position 4 is at five channel widths after the bend. As seen in Fig. 4, 1 μm particles tend to accumulate at the outer wall of the bend, which results in a very high particle density gradient. 5 μm particles also form a particle

Advances in Fluid Mechanics V, A. Mendes, M. Rahman & C. A. Brebbia (Editors)

density gradient at the outer wall, but it is comparatively small (See Fig. 5). When the particles travel along the straight channel, small particles are deposited on the wall due to diffusional deposition, and large particles are deposited due to eddy impaction and inertial deposition. When curvature exists in the flow, the particles' inertia causes the particles to deviate from the streamlines of the gas phase. In other words, when the particles are subjected to a flow-field with curvature, the centrifugal force drives the particles away from the centre of the curvature. To identify the effect of the curvature on particle deposition, the centrifugal force ***Fc*** is compared with the major driving force in deposition problems, the turbophoretic force ***Ft***:

$$\left|\frac{F_c}{F_t}\right| = \left|\frac{\dfrac{V_r^2}{r}}{\dfrac{\partial \overline{v_r' v_r'}}{\partial r}}\right| \tag{15}$$

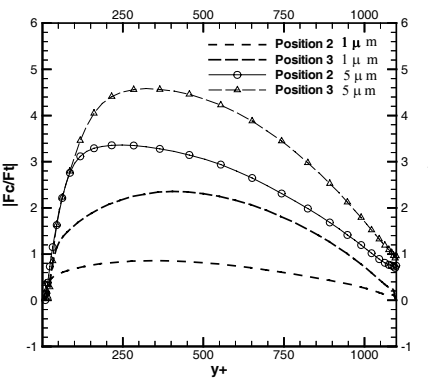

Figure 6.

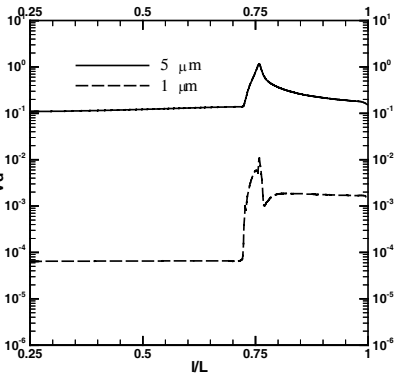

Figure 7.

The ratio of the two forces is shown in Fig. 6. It is seen that, even for 1 μm particles, the centrifugal force is comparable with the turbophoretic force at the bend. For 5 μm particles, the centrifugal force is larger at most parts of the bend, which means, the centrifugal effect will cause critical changes in the deposition rate. As the small particles (1 μm) move through the bend, they gradually translate towards the outer wall by the centrifugal force, but the inertia of the particle is not large enough for the particles to penetrate the turbulent boundary layer and arrive at the wall. Thus a high particle concentration is formed at the wall, which will contribute to the diffusion deposition. Large particles (5 μm) will simply translate towards the wall, penetrate the turbulent boundary layer and arrive at the wall. Fig. 7 shows the deposition rate for the particles. The deposition rate is defined as in eqn. (3), with the mean density taken as the average of that across the local cross section. The x coordinate is the length along the outer wall, normalized by the total outer wall length. The bend part is

Advances in Fluid Mechanics V, A. Mendes, M. Rahman & C. A. Brebbia (Editors)

between l/L=0.725-0.758. It is obvious that the 1 μm particles remain at a higher deposition rate after the bend. This is due to the high particle concentration that builds up near the wall at the bend. Though the deposition rate at the bend is greatly increased, the absolute value is still very low. Thus most particles that accumulate close to the outer wall will not deposit on the wall. They will move along with the flow, keeping the particle concentration high close to the outer wall, and contribute to a higher particle deposition rate after the bend.

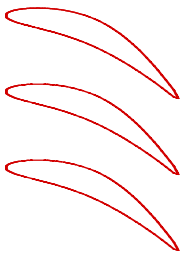

Figure 8.

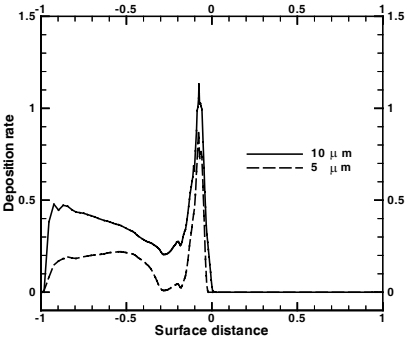

Figure 10.

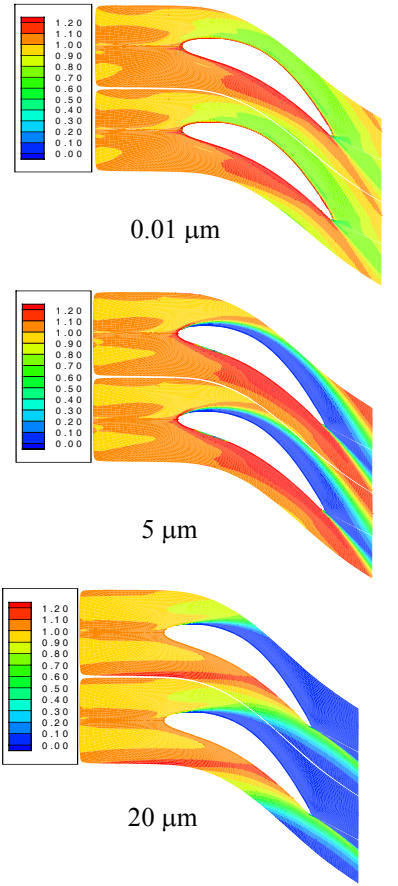

Figure 9.

5.3 Depostion from turbulent cascade flow

The geometry used for the calculation of gas-particle flows through a turbine cascade is that of the side-stream experiment from the British Coal project (Fackrell et al. [1]). The turbine blade cascade is shown in Fig. 8. The blade chord was 37 mm and the inlet temperature was 1500K, with maximum Mach

number of around 0.6. A 'C mesh' was generated around one of the blades, with periodic boundary conditions for the upper and the lower boundaries to represent a cascade situation. A fine grid was used close to the wall, and the grid became coarser as it moved away from the surface.

At present, reliable gas-phase turbulence quantities are still difficult to obtain from numerical simulations that use turbulent models other than LES/DNS. To fill the gap, a patching scheme was used. The mean gas flow-field and the friction velocity distribution were taken from a previous study. The eddy viscosity and the wall–normal fluctuating velocity were then patched using the same formula that was used for the turbulent channel flow. The patched flow-field was then read into the particle flow solver, ready for the simulation of particle deposition.

In the simulations, the particle material density was 1e3 kg/m**3. Spherical particles with three diameters: 0.01 μm, 5 μm and 10 μm were used.

Figure 9 shows the particle density contours for particles with different diameters. The smallest particles, 0.01 μm in diameter, occupy the whole flow-field, because they follow the gas phase well. Nevertheless, even for this size of particle, inertia plays an important role, since the particle density on the pressure side is higher than on the suction side. For 5 μm particles a particle free zone (where the particle density is zero) forms on the suction surface. For particles of this size, inertia effect and turbophoresis play equally important roles. Particle inertia alone is insufficient to make the particles penetrate the boundary layer and a high particle density is observed on the pressure side of the blade. 20 μm particles are large enough to ignore the turbulence, and they penetrate the turbulent boundary layer directly to arrive at the pressure surface of the turbine blade. The curvature of the gas streamlines has very little effect on the particle translational speed, so their direction changes only slightly, and a large particle-free zone forms on the suction surface of the blade.

Figure 10 shows the particle deposition rate. The x-co-ordinate is the dimensionless blade surface distance. The origin of this co-ordinate is the leading edge and is positive along the suction surface, negative along the pressure surface. The deposition rate is defined as the ratio of the wall mass flux and the averaged inlet mass flux:

$$V_d^+ = \frac{J_W}{J_{in}} \tag{16}$$

As seen in fig. 10, starting from the trailing edge, the particle deposition rates increase rapidly, and then drop down gradually. Right before the leading edge, the deposition rate rises again, and reaches its maximum. After that, the deposition rate drops down rapidly to almost zero. This shows that for particles with moderate inertia, the deposition will mainly happen on the pressure side of the turbine blade. On the suction side, the deposition occurs due to turbulent diffusion, but because of the very low particle concentration, the rate is very low.

Advances in Fluid Mechanics V, A. Mendes, M. Rahman & C. A. Brebbia (Editors)

6 Concluding remarks

Particle depositions from different turbulent flows have been studied. A 2-D particle deposition code has been used to simulate a well-defined and well-researched case, namely deposition from turbulent channel flows. The deposition curve calculated by the 2-D code agrees well both with the results of a 1-D code and a variety of experimental data. The effect of curvature on deposition has been studied on a turbulent bent duct. The results show that curvature has a great effect on the distribution of particle density and the particle deposition rate. This effect is observed even for very small particles (τ_p^+=0.64). The study has been extended to the problem of deposition in a cascade of turbine blades. Reasonable results have been obtained. These studies show the possibility of using the current method on industrial deposition problems.

Acknowledgement

The work was sponsored by DTI, Rolls Royce and PowerGen. The authors wish to thank Dr. John Fackrell of PowerGen for his support.

References

[1] Fackrell, J.E., et al., 1994, 'Modelling Particle Deposition in Gas Turbines Employed in Advanced Coal-Fired Systems', *Int. Gas Turbine and Aeroengine Congress*, The Hague, The Netherlands, Paper 94-6T-467.
[2] Hinze, J.O., 1975, 'Turbulence', New York: McGraw-Hill.
[3] Leeming, A. D., 1996, 'Particle deposition from turbulent flows', PhD thesis, Cambridge University Engineering Department.
[4] Simonin, O. and Viollet, P.,L., 1990, ' Modeling of Turbulent Two-Phase Jets Loaded with Discrete Particles', *Interface phenomenon in multi-phase flow, Dubrovnik, Ed. G. F. Hewitt, Hemisphere*
[5] Slater, S.A., Leeming, A.D. & Young, J.B., 2003, 'Particle deposition from two-dimensional turbulent gas flows', *Int. J. Multiphase Flow.*
[6] Slater, S.A. & Young, J.B., 2001, 'The calculation of inertial particle transport in dilute gas-particle flows', *Int. J. Multiphase Flow,* **27,** 61-87.
[7] Young, J.B. & Leeming, A.D., 1997, 'A theory of particle deposition in turbulent pipe flow', *J. Fluid Mech.*

Advances in Fluid Mechanics V, A. Mendes, M. Rahman & C. A. Brebbia (Editors)